Bull. Mater. Sci., Vol. 35, No. 3, June 2012, pp. 377–382. © Indian Academy of Sciences.

Fabrication of nano-sized solid solution of $Zn_{1-x}Mn_xO$ ($x = 0{\cdot}05, 0{\cdot}10, 0{\cdot}15$) in reverse microemulsions: Structural characterization and properties

SARVARI KHATOON, APARNA GANGULY and TOKEER AHMAD*
Department of Chemistry, Jamia Millia Islamia, New Delhi 110 025, India

MS received 4 July 2011; revised 25 August 2011

Abstract. **Mn-doped ZnO nanoparticles were synthesized by reverse micellar method using Tergitol NP9 as a surfactant for the first time. These nanoparticles were characterized using powder X-ray diffraction, transmission electron microscopy and selected area electron diffraction analysis. Structural analysis and optical studies revealed that manganese is incorporated into the ZnO host lattice forming a solid solution. Transmission electron microscopic studies show that the particle size increases from 20–50 nm on increasing the dopant concentration from 0·05–0·15. The specific surface area of $Zn_{1-x}Mn_xO$ ($x = 0{\cdot}05$, 0·10 and 0·15) as calculated using BET method was found to be 202·62, 145·78 and 75·66 m^2g^{-1}, respectively which are higher than the reported values so far.**

Keywords. **Reverse micelle; solid solution; electron microscopy; surface area.**

1. Introduction

Dilute magnetic semiconductors (DMSs) have attracted considerable attention because of the possibility of incorporating degrees of freedom (charge and spin) in a single material, which results in a new class of devices known as spintronics (spin transfer electronics) (Ohno 1998; Diet *et al* 2000; Matsumoto *et al* 2001; Ogale *et al* 2003; Pearton *et al* 2003). Zinc oxide is an *n*-type semiconductor with a wide bandgap (3·4 eV) and large excitonic binding energy of 60 meV at room temperature. Due to its outstanding physical and chemical properties, ZnO appears to be an exceptionally important host material for the envisaged applications in many technologies, such as solar energy conversion and optoelectronic devices (Zhang *et al* 2002). Solid solution of Mn-doped ZnO nanoparticles has shown potential applications in the field of short-wave magneto-optical devices (Zaets and Ando 2000).

Numerous techniques have been used for the synthesis of Mn-doped ZnO solid solution, such as co-precipitation (Joseph *et al* 2005), hydrothermal (Yang *et al* 2010), sol–gel (Kim *et al* 2004), combustion method (Luo *et al* 2005), autocombustion method (Deka and Joy 2007), rheological phase reaction precursor method (Cong *et al* 2005) and other physical methods. Among the chemical methods, reverse micellar method is a versatile method which does not require any specialized or expensive equipments for obtaining uniform, homogenous and monodisperse nanoparticles of wide ranging compositions (Ahmad *et al* 2004, 2006; Ahmad and Ganguli 2004, 2006). The reverse micelles act as nanoreactors which determine the size and shape of nanoparticles and also inhibit the excess aggregation of particles (Luisi and Magid 1986; Pileni 1989; Paul and Moulik 1997). The formation of particles in reverse micelles can be achieved by using either a single-microemulsion or multiple microemulsions depending on the composition. In the single-microemulsion approach, one microemulsion is prepared, and the precursor or reactant is then added, diffusing through the oil phase into the micelles. The second process, viz. the multimicroemulsion route, takes advantage of two or more separately prepared microemulsions of the same water/surfactant/oil ratio, differing only in their aqueous content. There are only few reports that are available in the literature for the synthesis of Mn-doped ZnO nanoparticles using reverse micellar method (Jayakumar *et al* 2007).

In this paper, we report the synthesis, characterization and optical properties of Mn-doped ZnO solid solutions by reverse micellar method using tergitol as a surfactant for the first time. The nanoparticles have been characterized by powder X-ray diffraction, transmission electron microscopy and BET surface area analysis. Optical properties of these particles have also been measured.

2. Experimental

0·1 M solutions of Zn^{2+}, Mn^{2+} and NaOH were prepared in double distilled water from zinc acetate dihydrate (CDH, 98·5%), manganese acetate tetrahydrate (CDH, 99%), and sodium hydroxide (Qualigens, 97%), respectively. The synthesis procedure for $Zn_{1-x}Mn_xO$ ($x = 0{\cdot}05$, 0·10 and 0·15)

*Author for correspondence (tokeer.ch@jmi.ac.in)

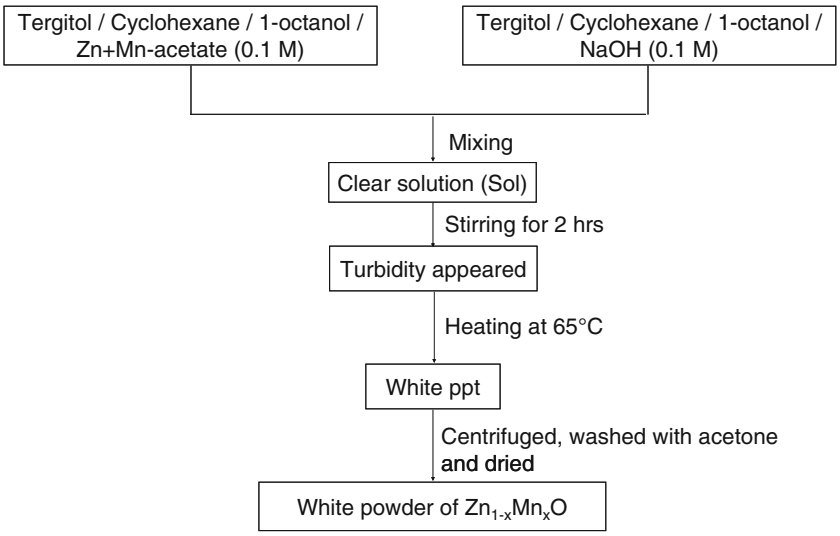

Figure 1. Flowchart for reverse micellar synthesis of Mn-doped ZnO nanoparticles.

involves the use of two different microemulsions (I and II), one for metal ions and the other for the precipitating agent. 21 mL tergitol NP-9 (Aldrich), 15·6 mL 1-octanol (Loba Chemie, 99%), 180 mL cyclohexane (Rankem, 99·5%) as non-polar solvent and 9 mL aqueous phase containing metal salts of Zn^{2+} and Mn^{2+} were the constituents of the microemulsion I. The stoichiometry of the metal salts was maintained according to the stoichiometry of the dopant. In microemulsion II, all the constituents remain same except the aqueous phase (0·1 M NaOH), which is used for precipitating the metal ions. These two microemulsions were mixed slowly and stirred at room temperature for 2 h. A transparent solution was obtained from which the solvent was evaporated at 60 ± 5°C. A white precipitate was obtained. The product was collected by centrifugation and washed several times with acetone and then dried in an oven at 50°C. The as-prepared samples were annealed in air at 500°C for 6 h and finally at 700°C for 12 h. The flowchart for the synthesis of Mn-doped ZnO i.e. $Zn_{1-x}Mn_xO$ ($x = 0{\cdot}05$, 0·10 and 0·15) solid solutions using reverse micellar method is shown in figure 1.

The samples were characterized using a Bruker D8 Advance X-ray diffractometer with Ni-filtered Cu-Kα radiation. Normal scans were recorded with a step size of 0·05° and step time of 1 s. The size and morphology have been studied by transmission electron microscopy (TEM) using FEI Technai G^2 20 transmission electron microscope with an accelerating voltage of 200 kV. TEM specimens were prepared by dispersing the samples in ethanol and placing a drop of the dispersed samples in a copper grid. Room temperature optical properties were confirmed by a UV-visible spectrophotometer (Ocean Optics Lambda-25). N_2 adsorption studies were carried out on a Quantachrome NOVA 2000e instrument using the BET method to determine the surface area. Samples were degassed at 250°C for 3 h in vacuum for the removal of any adsorbed gases. After degassing, specific surface areas were obtained from the nitrogen adsorption experiments measured at 77·35 K.

3. Results and discussion

3.1 *Powder X-ray diffraction (PXRD) studies*

PXRD patterns of all the Mn-doped (i.e. 5%, 10% and 15% by weight) ZnO show the formation of zincite (hexagonal) phase with slight shifting as shown in figure 2. The reflections could be indexed on the basis of hexagonal crystal lattice (JCPDS No. 750576, lattice parameters: 3·242 Å and 5·194 Å). The room temperature Mn-doped samples at 5 wt %, 10 wt % and 15 wt % concentrations showed one impurity peak of Mn_2O_3 which has been marked by asterisks. However, this impurity is diminished on heating the samples at high temperatures (700°C). Similar behaviour is recently reported for $Mn_{0{\cdot}50}Zn_{0{\cdot}50}Fe_2O_4$ in which Fe_2O_3 and Mn_2O_3 were dissolved after annealing at 1100°C (Hu *et al* 2010). The crystallinity increases on increasing the sample temperature. The cell parameters were refined using the CELL software and it was found that at room temperature with increasing Mn content the '*a*' lattice parameter does not show any significant difference, although a minor change could be seen in the '*c*' lattice parameter. At higher temperature i.e. 700°C, the lattice parameter '*a*' shows a slight increase in its value from 3·249(7) to 3·256(6) Å, however, the '*c*' lattice parameter shows a change from 5·19(2) to 5·20(2) Å. Thus, all the diffraction patterns indexed to the pure ZnO phase with slight shift of the diffraction peaks correspond to the formation of solid solution of Mn–ZnO system.

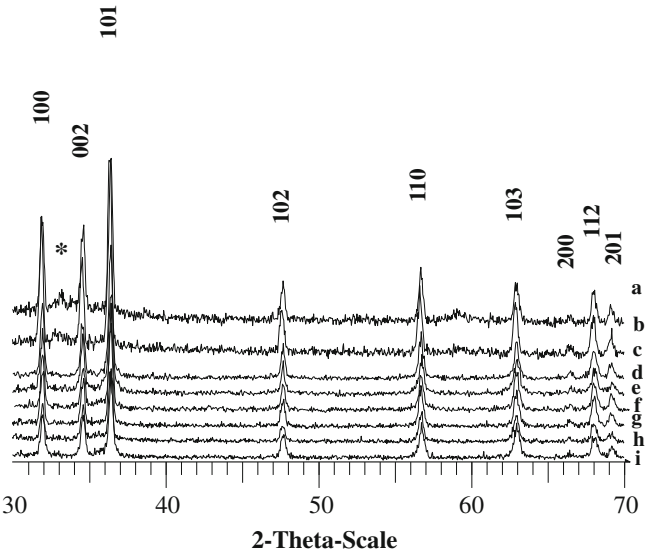

Figure 2. Powder X-ray diffraction pattern of $Zn_{1-x}Mn_xO$ nanoparticles for $x =$ (**a**) 0·05, (**b**) 0·10, (**c**) 0·15 at room temperature, (**d**) 0·05, (**e**) 0·10, (**f**) 0·15 heated at 500°C, (**g**) 0·05, (**h**) 0·15 and (**i**) 0·10 heated at 700°C.

3.2 *FTIR spectral studies*

FTIR spectrum of as prepared Mn-doped ZnO nanoparticles at room temperature in the range of 500–3900 cm^{-1} is shown in figure 3(a-c). The IR spectrum shows a strong band centred at about 3332 cm^{-1} corresponding to the stretching vibrations of –OH groups and band at around 1573 cm^{-1} attributed to the bending vibration of adsorbed molecular water (Sibu *et al* 2002). The weak bands appeared around 1388 cm^{-1} are attributed to the bending vibration of $–CH_2$ (MacPhail *et al* 1984) which arise due to the association of surfactant molecules with Mn-doped ZnO. The bands observed at around 830 cm^{-1} and below are assigned to the metal oxide M–O bond as present in Zn–O and Mn–O. All the bands above 1500 cm^{-1} disappeared on heating the samples at 500°C in order to eliminate water molecules and other adsorbed impurities (figure 3(d-f)). On further heating the samples at 700°C, the only band observed is below 700 cm^{-1} which corresponds to the metal oxide bond as shown in figure 3(g-i) which confirms formation of pure Mn-doped ZnO solid solution.

3.3 *Transmission electron microscopic (TEM) studies*

Figure 4 shows TEM micrographs of $Zn_{1-x}Mn_xO$ ($x = 0{\cdot}05$, 0·10 and 0·15). TEM image of $Zn_{0.95}Mn_{0.05}O$ shows hexagonal geometry of nanoparticles. The particle size lies in the range of 15–25 nm with an average particle size of 20 nm. The particles are uniform in size as seen from figure 4a. Figure 4b shows TEM image of $Zn_{0.90}Mn_{0.10}O$ nanoparticles in which cuboidal nanoparticles are seen along with hexagonal particles of size 25 nm. On further increasing the dopant concentration from 0·10–0·15, the average size of hexagonal nanoparticles increases from 25–50 nm. TEM micrograph (figure 4c) gives the bimodal distribution of nanoparticles with average sizes of 9 nm and 50 nm. The larger particles are of hexagonal geometry, whereas the smaller particles are in spherical shape. It is clear from the image that the smaller particles are trying to agglomerate to form the bigger hexagonal shaped nanoparticles. Thus on increasing the dopant concentration from 0·05–0·15, we observe an increase in the average particle size from

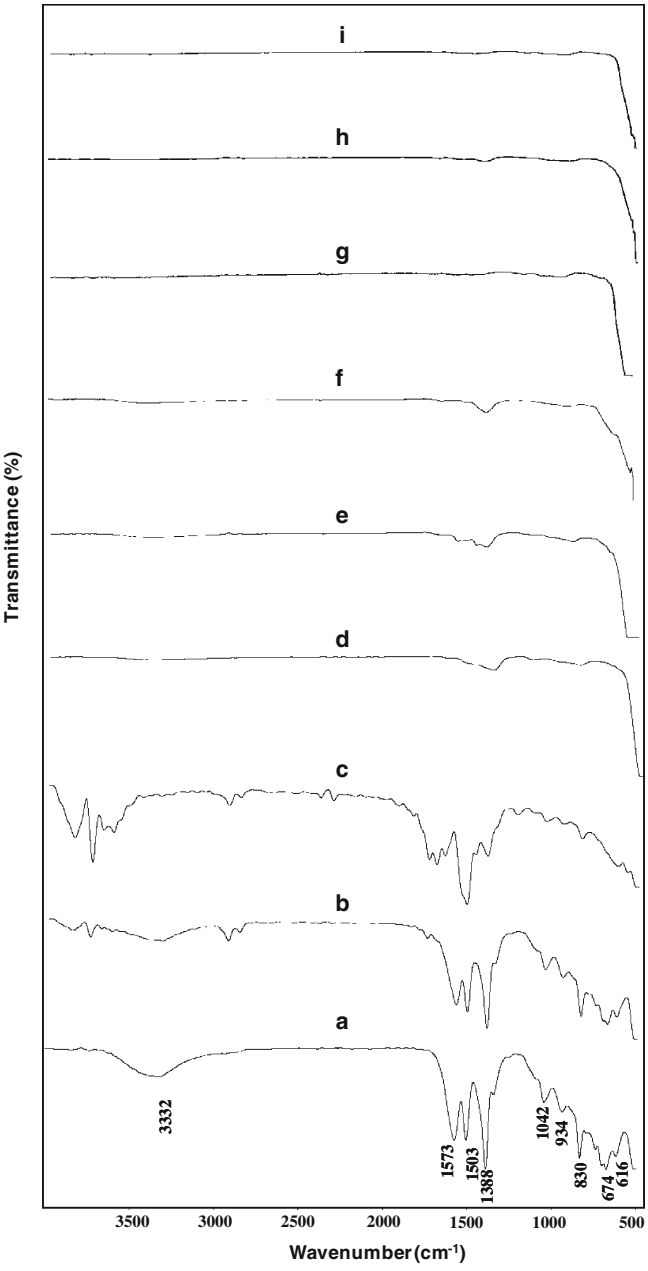

Figure 3. FTIR spectrum of $Zn_{1-x}Mn_xO$ nanoparticles for $x =$ (**a**) 0·05, (**b**) 0·10, (**c**) 0·15 at room temperature, (**d**) 0·05, (**e**) 0·10, (**f**) 0·15 heated at 500°C, (**g**) 0·05, (**h**) 0·10 and (**i**) 0·15 heated at 700°C.

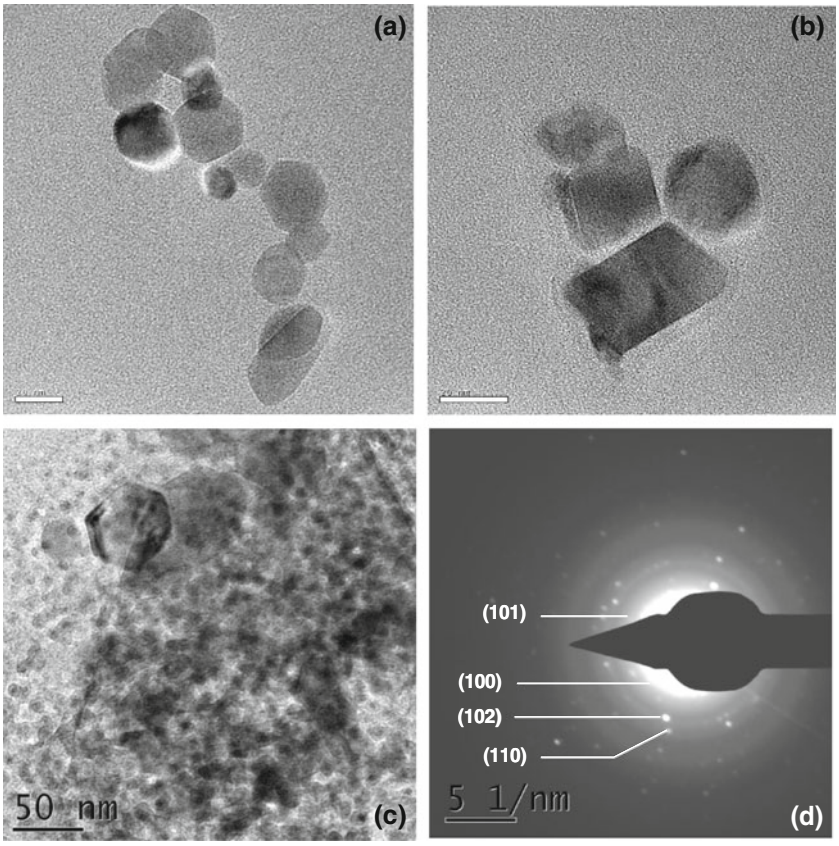

Figure 4. TEM micrographs of $Zn_{1-x}Mn_xO$ solid solution at (**a**) $x = 0{\cdot}05$, (**b**) $x = 0{\cdot}10$ and (**c**) $x = 0{\cdot}15$, and (**d**) SAED of $Zn_{0{\cdot}85}Mn_{0{\cdot}15}O$ nanoparticles.

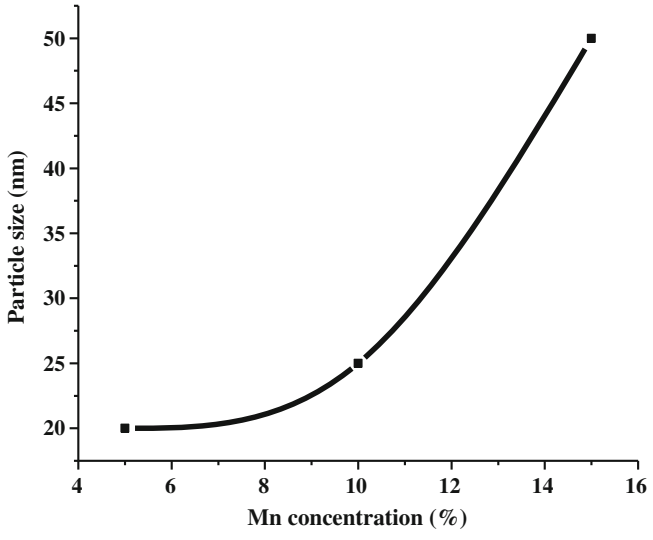

Figure 5. Plot of variation of particle size vs manganese concentration.

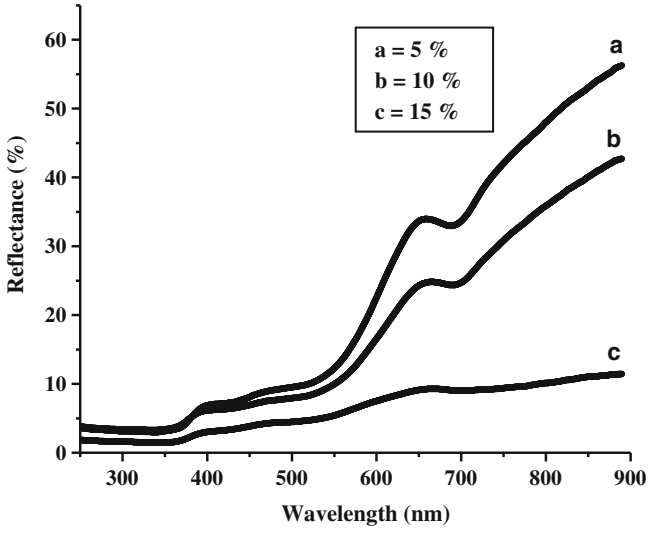

Figure 6. UV-visible reflectance spectra of $Zn_{1-x}Mn_xO$ nanoparticles for $x =$ (**a**) 0·05, (**b**) 0·10 and (**c**) 0·15 heated at 700°C.

20–50 nm as shown in figure 5. This may be attributed to the possibility of agglomeration of the particles due to more amount of Mn (15%) in the loaded composition. Figure 4d shows selected area electron diffraction (SAED) of $Zn_{0·85}Mn_{0·15}O$ nanoparticles. The diffraction rings show the nanocrystalline nature of the solid solution and corresponds to the interplanar distances of 2·21, 2·77, 1·63 and 1·84 Å which are in good agreement with the planes (101), (100), (110) and (102), respectively for hexagonal ZnO. Similar SAED pattern was observed for the compositions of $Zn_{0·95}Mn_{0·05}O$ and $Zn_{0·90}Mn_{0·10}O$ (not shown).

3.4 *Optical properties*

Discs of Mn-doped ZnO nanoparticles (heated at 700°C) were made to measure the optical properties. Reflectance spectra of these samples were carried out in the range of 250–900 nm at room temperature as shown in figure 6. Reflectance spectra show three absorption peaks. First absorption band appeared at around 420 nm which is red shifted to undoped ZnO. These nanoparticles gave a broad absorption band in the range of 440–510 nm which is due to the ${}^6A_1(S) \rightarrow {}^4T_1(G)$ transition at Mn^{2+} sites (Rao and Deepak 2005). Third absorption peak appeared at ∼680 nm corresponding to the ${}^4T_1 \rightarrow {}^4A_2$ transition of Mn^{2+} which arises due to 3*d*–3*d* electron transitions (Yang *et al* 2002; Denisov *et al* 2003). On increasing the dopant concentration, the spectra shifted towards the lower wavelength which indicates that the bandgap increases on increasing the Mn concentration. This behaviour is explained by the Burstein–Moss effect (Suwanboon *et al* 2007). Thus reflectance studies confirmed that manganese is in divalent state.

3.5 *BET surface area studies*

The Brunauer–Emmett–Teller (BET) gas adsorption method was used for the determination of the surface area (Brunauer *et al* 1938) and the pore size distribution (pore radius and pore volume) was calculated using Barrett–Joyner–Halenda (BJH) method (Barrett *et al* 1951). Figure 7 shows BET plots of $Zn_{1-x}Mn_xO$ ($x = 0·05$, 0·10 and 0·15) nanoparticles heated at 700°C. The specific surface area of these nanoparticles calculated using the BET equation comes out to be 202·62, 145·78 and 75·66 m^2g^{-1}, respectively which are found to be higher than the reported value so far. Pore size distribution plot of these solid solutions is shown in figure 8. The pore radius of these nanoparticles as calculated using BJH was found to be 15·22, 15·35 and 17·19 Å, respectively with the corresponding pore volumes of 4·09, 3·78 and 0·79 cm^3g^{-1}. The observed variation in surface area and pore size can be correlated to the increase in the particle size on increasing the dopant concentration. The average particle size of these nanoparticles can also be estimated by assuming the particles to have spherical shape and smooth surface using the equation (Li *et al* 2003),

$$D_{\mathrm{BET}} = 6000/(\rho.S_{\mathrm{w}})$$

where D_{BET} is the average diameter of the particle in nm; ρ the density in gcm^{-3} and S_{w} the measured surface area of nanoparticle in m^2g^{-1}. The particle size calculated using the above equation comes out to be 5, 7 and 14 nm, respectively (table 1). These results show that particle size increases on decreasing the surface area. However, the particle size is low in comparison to that obtained by TEM studies. The difference in TEM and BET particle sizes may be attributed to the fact that during BET experiment there is removal of adsorbed impurities by degassing the samples and

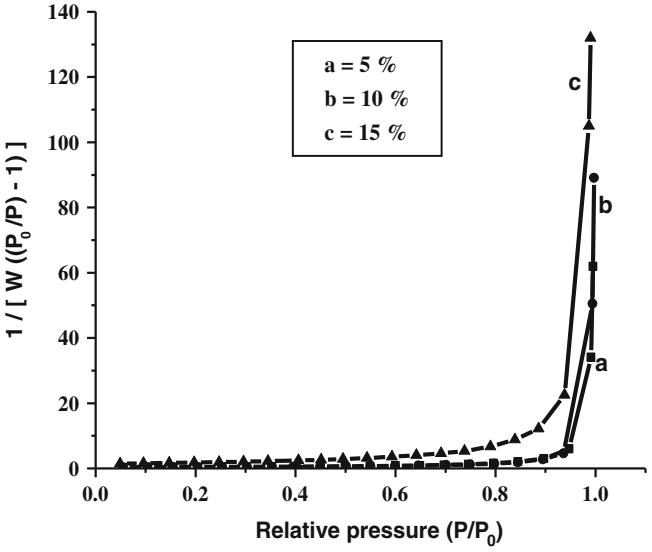

Figure 7. BET plot of $Zn_{1-x}Mn_xO$ nanoparticles for $x =$ (**a**) 0·05, (**b**) 0·10 and (**c**) 0·15 heated at 700°C.

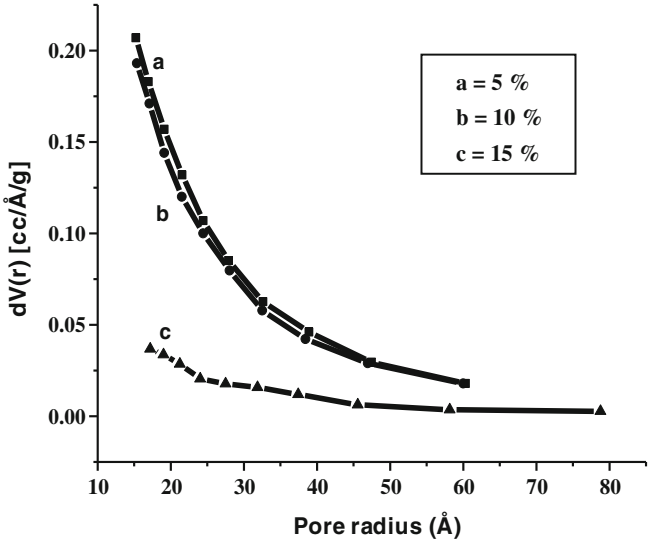

Figure 8. BJH plot of $Zn_{1-x}Mn_xO$ nanoparticles for $x =$ (**a**) 0·05, (**b**) 0·10 and (**c**) 0·15 heated at 700°C.

Table 1. BET surface area, BJH pore size distribution and particle size of $Zn_{0.95}Mn_{0.05}O$, $Zn_{0.90}Mn_{0.10}O$, and $Zn_{0.85}Mn_{0.75}O$ nanoparticles heated at 700°C.

Sample		$Zn_{0.95}Mn_{0.05}O$	$Zn_{0.90}Mn_{0.10}O$	$Zn_{0.85}Mn_{0.15}O$
BET surface area $[m^2g^{-1}]$		202·62	145·78	75·66
BJH	Pore radius [Å]	15·22	15·35	17·19
	Pore volume [cc/Å/g]	4·09	3·78	0·79
Particle size (nm)	TEM	20	25	50
	BET surface area	5	7	14

agglomeration may be attained in TEM studies during sample preparation.

4. Conclusions

Nanocrystalline Mn-doped ZnO (5%, 10% and 15% by weight) solid solutions have been successfully synthesized by the reverse micellar method using tergitol as the surfactant for the first time. The phase purity of the solid solutions was further confirmed by the FTIR studies. TEM studies show that the particle size increases from 20–50 nm on increasing the manganese concentration from 0·05–0·15 which may be attributed to the large amount of agglomeration. UV-Visible reflectance spectra shows a broad absorption in the range of 440–510 nm that corresponds to the $^6A_1(S) \rightarrow {}^4T_1(G)$ transition at Mn^{2+} sites which confirmed that manganese is in divalent state. Specific surface area of these nanoparticles was found to be 202·62, 145·78 and 75·66 m^2g^{-1}, respectively which are found to decrease with increasing particle size.

Acknowledgements

One of the authors (TA) thanks CSIR, Govt. of India, for financial support of the research project (No. 01(2448)/10EMR-II). The authors also thank DST for funding installation of HRTEM facility at IIT Delhi. (SK) thanks UGC and CSIR for research fellowships.

References

Ahmad T and Ganguli A K 2004 *J. Mater. Res.* **19** 2905
Ahmad T and Ganguli A K 2006 *J. Am. Ceram. Soc.* **89** 3140
Ahmad T, Ramanujachary K V, Lofland S E and Ganguli A K 2004 *J. Mater. Chem.* **14** 3406
Ahmad T, Vaidya S, Sarkar N, Ghosh S and Ganguli A K 2006 *Nanotechnology* **17** 1236
Barrett E P, Joyner L G and Halenda P P 1951 *J. Am. Chem. Soc.* **73** 373
Brunauer S, Emmett P H and Teller E 1938 *J. Am. Chem. Soc.* **60** 309
Cong C J, Liao L, Li J C, Fan L X and Zhang K L 2005 *Nanotechnology* **16** 981
Deka S and Joy P A 2007 *Solid State Commun.* **142** 190
Denisov A, Volk Y V, Malyarevich A M, Yumashev K V, Dymshits O S, Zhilin A A, Kang U and Lee K 2003 *J. Appl. Phys.* **93** 3827
Diet T, Ohno H, Matsukura F, Cibert J and Ferrand D 2000 *Science* **287** 1019
Hu P, Yang H, Pan D, Wang H, Tian J, Zhang S, Wang X and Volinsky A A 2010 *J. Magn. Magn. Mater.* **322** 173
Jayakumar O D, Gopalakrishnan I K, Kadam R M, Vinu A, Asthana A and Tyagi A K 2007 *J. Cryst. Growth* **300** 358
Joseph D P, Kumar G S and Venkateswaran C 2005 *Mater. Lett.* **59** 2720
Kim Y M, Yoon M, Park I-W, Park Y J and Lyou J H 2004 *Solid State Commun.* **129** 175
Li J G, Ikegami T, Wang Y and Mori T 2003 *J. Am. Ceram. Soc.* **86** 915
Luisi P L and Magid L J 1986 *CRC Crit. Rev. Biochem.* **20** 409
Luo J, Liang J K, Liu Q L, Liu F S, Zhang Y, Sun B J and Rao G H 2005 *J. Appl. Phys.* **97** 086106
MacPhail R A, Strauss H L and Snyder R G 1984 *J. Phys. Chem.* **88** 334
Matsumoto Y *et al* 2001 *Science* **291** 854
Ogale S B *et al* 2003 *Phys. Rev. Lett.* **91** 077205
Ohno H 1998 *Science* **281** 951
Paul B K and Moulik S P 1997 *J. Dispersion Sci. Technol.* **18** 301
Pearton S J, Abernathy C R, Norton D P, Hebard A F, Park Y D, Boatner L A and Budai J D 2003 *Mater. Sci. Eng.* **R40** 137
Pileni M P (ed.) 1989 *Structure and reactivity in reverse micelles* (Amsterdam: Elsevier)
Rao C N R and Deepak F L 2005 *J. Mater. Chem.* **15** 573
Sibu C P, Kumar S R, Mukundan P and Warrier K G K 2002 *Chem. Mater.* **14** 2876
Shannon R D 1976 *Acta Crystallogr.* **A32** 751
Suwanboon S, Ratana T and Ratana W T 2007 *J. Sci. Technol.* **4** 111
Yang S G, Pakhomov A B, Hung S T and Wong C Y 2002 *IEEE Trans. Magn.* **38** 2877
Yang T, Li Y, Zhu M Y, Li Y B, Huang J, Jin H M and Hu Y M 2010 *Mater. Sci. & Engg.* **B170** 129
Zaets W and Ando K 2000 *Appl. Phys. Lett.* **77** 1593
Zhang X T *et al* 2002 *J. Appl. Phys.* **92** 3293